Available online at www.sciencedirect.com
ScienceDirect
Proceedings of the Combustion Institute 000 (2020) 1–8
Proceedings of the Combustion Institute
www.elsevier.com/locate/proci

Self-excited longitudinal and azimuthal modes in a pressurised annular combustor

Marek Mazur [a,*], Yi Hao Kwah [b], Thomas Indlekofer [b], James R. Dawson [b], Nicholas A. Worth [b]

[a] *CORIA-UMR 6614 Normandie Université, CNRS-Université et INSA de Rouen, Campus Universitaire du Madrillet, Saint Etienne du Rouvray, France*
[b] *Department of Energy and Process Engineering, Norwegian University of Science and Technology, Kolbjørn Hejes v 1B, 7491 Trondheim, Norway*

Received 7 November 2019; accepted 29 May 2020
Available online xxx

Abstract

A new laboratory scale pressurised annular combustion experiment is introduced and used to generate self-excited longitudinal and azimuthal instabilities. The experiments are operated at mean pressures ranging from approximately 2 to 3 atmospheres in order to maintain a well defined acoustic boundary at exit. A range of operating conditions is studied parametrically, and it is observed that at high equivalence ratios, the flame stabilisation location propagates upstream, significantly altering the flame structure. The change in flame stabilisation location promotes a transition from a dominant longitudinal to a dominant azimuthal instability. Investigation of the azimuthal instabilities highlights a rich array of frequency content, with significant amplitude pressure and heat release responses observed for not only the fundamental ($n = 1$), but also higher harmonics ($n = 2, 3$). These higher harmonics are also shown to exhibit distinct characteristic modal dynamics, shown through probability density functions of the spin ratio. The flame dynamics for three distinct operating states, corresponding to longitudinal modes at two different stabilisation locations, and one corresponding to strong azimuthal modes are studied. These highlight the difference between longitudinal and azimuthal modes, and demonstrate the presence of significant higher harmonic content. The characterisation of both longitudinal and azimuthal modes in a pressurised laboratory scale annular combustor for the first time provides a unique opportunity for understanding the nature of such instabilities in practically relevant configurations.

Keywords: Pressurised combustor; Combustion instability; Annular combustor; Azimuthal modes; Flame dynamics

1. Introduction

Thermoacoustic instabilities remain an important issue for the design and operation of aero

* Corresponding author.
E-mail address: marek.mazur@coria.fr (M. Mazur).

https://doi.org/10.1016/j.proci.2020.05.033

engines and stationary gas turbines. Many engines utilise annular combustion chambers, which may experience self-excited azimuthal modes [1]. The ability to replicate azimuthal instabilities in both lab and industrial scale annular combustors has given way to a range of recent experimental [2–7], numerical [8,9], and theoretical studies [10–14], which have provided insight into their nature. These have shown that the dominant mode shapes and modal dynamics (referring to the time-varying spin ratio, orientation, and strength of a mode) are associated with parameters such as burner geometry, equivalence ratio, bulk velocity, the presence or absence of a mean azimuthal flow, as well as whether the fuel is gaseous or liquid.

In previous experimental studies, however, the boundary conditions were not always well defined. In particular the acoustic impedance at the exit of the annular combustion chamber, which is commonly open to atmosphere [3,4]. As described in [3], depending on the length ratio between the inner and outer chamber walls, the combustor exhibits longitudinal and/or azimuthal modes, highlighting the importance of the downstream acoustic boundary. A similar combustor height mismatch was also employed by Bourgouin et al. [4] to generate azimuthal modes, with strong acoustic activity in the plenum showing the importance of the upstream boundary conditions. These boundary conditions are not trivial to replicate numerically, so simpler, more practically relevant conditions are necessary.

One way to generate a well-defined downstream boundary condition is to choke the flow; a condition which implies the pressurisation of the combustor ($\gtrapprox$200 kPa). Due to the additional complexity and cost of such configurations, most studies have been conducted on pressurised single flames. Such studies have shown that an increase in combustor pressure leads to more compact flames [15], the modified acoustic boundary conditions can exert a strong influence on the mode structure [16,17], and can generate extremely large pressure oscillations, resulting in phenomena such as acoustically induced flashback [18]. While studies have featured annular combustion chamber geometry under pressurised conditions [19], many of these are in practical devices with highly complex geometry and limited optical access. While pressurised measurements in a lab scale annular combustor have been reported previously [20], only forced rather than self-excited oscillations have been observed.

The aim of the current investigation is to investigate self-excited azimuthal modes which occur in a pressurised lab scale annular combustor, during flame flashback. Choking the flow replicates the important acoustic boundary conditions of practical devices, allowing the effect of the boundary condition on the instabilities to be better understood. Furthermore, well-defined acoustic boundaries will help future simulations to replicate such experimental results, significantly enhancing our understanding. The remainder of the paper introduces a new experimental setup which allows both self-excited longitudinal and azimuthal modes to be studied for the first time at elevated pressure in a laboratory scale burner. In the current setup, azimuthal modes are only excited after flame flashback, which in itself is a phenomenon of significant interest. Therefore, the occurrence and transitional behaviour of these modes is discussed and the overall system stability and flame dynamics are described. Finally some conclusions are drawn.

2. Experimental methods

2.1. Intermediate Pressure Annular (IPA) combustor

Experiments were carried out in a novel Intermediate Pressure Annular (IPA) model combustor, shown schematically in Fig. 1. The flow geometry largely replicates that of previously reported atmospheric annular setups [2,3], with the addition of a convergent nozzle to choke the flow at the exit.

A premixed ethylene-air mixture is passed through a cylindrical plenum containing steel wool and glass beads to improve flow uniformity. The flow divides around a hemispherical bluff body, and is passed through a 22 mm thick sintered metal plate (mean pore size 183 μm, porosity 0.12, and $\Delta p = 15$ kPa). The acoustic boundary between the sintered metal plate and injection tubes was determined experimentally, and is characterised in the supplementary material.

The flow is divided between 12 injector tubes of $D_{inj} = 19$ mm, resulting in a non-dimensional flame separation distance of $S/D_{inj} = 2.3$. Each injector tube contains a central rod ($d_r = 5$ mm), which expands linearly at an angle of 38° over a stream-wise distance of 10 mm, resulting in a final bluff body of diameter $D_{bb} = 13$ mm. A six vane axial swirler, with the same geometry as reported previously [3], was positioned 10 mm upstream of the dump plane.

At the combustor exit, a first area reduction takes place through a symmetric matched 5th order contraction of length $L_{CR,1} = 34$ mm, and contraction ratio $CR = 7$, followed by a second area reduction via a replaceable blockage plate, with a thickness of 3 mm, featuring 164 holes of 2 mm diameter, distributed equally around a circle matching the mean chamber diameter $D_n = 169.5$ mm. This configuration mimics the approximately annular contraction in practical devices, resulting in a total area contraction ratio of $CR_{total} = 44$.

Main air and fuel flow rates were controlled using Mass Flow Controller (MFC) devices. Two MFCs (0 - 106.3 g/s) were used for air, and one MFC (0 - 20.7 g/s) was used for fuel. Each MFC was accurate to 0.8% of the reading plus ±0.2% of the full scale. The mean reactant supply tem-

Please cite this article as: M. Mazur, Y.H. Kwah and T. Indlekofer et al., Self-excited longitudinal and azimuthal modes in a pressurised annular combustor, Proceedings of the Combustion Institute, https://doi.org/10.1016/j.proci.2020.05.033

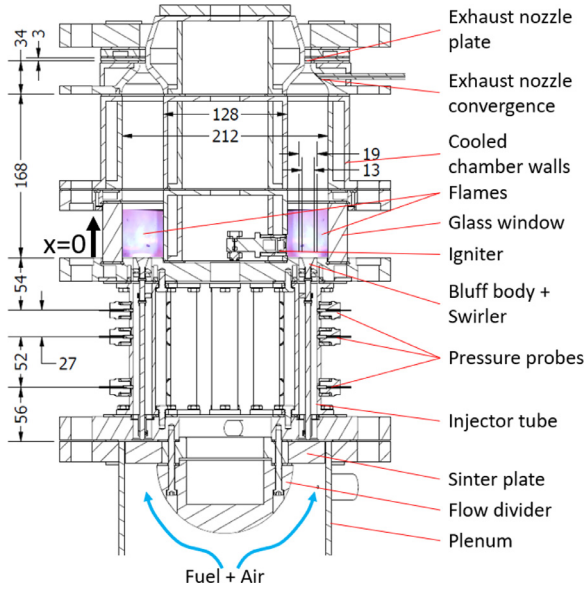

Fig. 1. Intermediate Pressurised Annular (IPA) combustor schematic with labels describing the main geometry and dimensions.

perature was around 293 K. A small independently operated pilot flame mounted on the inner annular wall was used to ignite the experiment. A range of equivalence ratios, $\phi = 0.65 - 0.95$, and air mass flow rates, $\dot{m}_a = 95.7 - 116.9$ g/s, was investigated.

Optical access was obtained through the outer annular wall as shown in Fig. 1. Three separate water paths were used to cool all other combustor surfaces, with isolated circuits for: 1. the dump plane; 2. the inner annular walls and inner nozzle walls; and 3. the outer annular walls and outer nozzle walls. A constant wall cooling flow rate was maintained in the three paths, which led to a combined cooling rate up to 80 kW.

2.2. Experimental measurements

Pressure fluctuations were measured in the injector tubes at three locations $x = -54$, -81, -133 mm upstream of the dump plane, at three angular locations around the annulus, $\theta_{k=\{1,2,3\}} = \{0°, 120°, 240°\}$. Pressure signals (from Kulite XCE-093 sensors, 1.4286×10^{-4} mV/Pa) were amplified (Fylde FE-579-TA) and sampled at $f_s = 51.2$ kHz during ~ 60 s for each experiment. The data presented in §3 corresponds to ~ 10 s for each run. Signals were digitised using a 24-bit DAQ system (NI model 9174). Each operating condition was tested 5 times, resulting in 175 experiments. Further to this, the transient case studied in Section 3.2 was tested 15 times to assess repeatability.

During experiments both longitudinal and azimuthal modes were observed, with the latter found to contain significant harmonics. To separate harmonic components, frequency-domain filtering is performed selectively using an Infinite Impulse Response (IIR) filter, with width $\Delta f_{filt} = 0.2$ kHz and $\Delta f_{filt} = 1$ kHz for longitudinal and azimuthal modes respectively.

Longitudinal pressure oscillation amplitudes are evaluated at the fundamental frequency, f_L, averaged over the three angular locations, and described through the term $P'_L = |p(f_L)'|$. Components of the azimuthal mode of order $n = 1 - 3$ are evaluated at frequencies $f_{A,n=\{1,2,3\}}$, with these herein referred to as the fundamental, and first and second harmonic components. The modal dynamics of the filtered azimuthal components are evaluated using the approach described previously [5,8], applied now to components of order n. Estimates are made for $A_+(n)$ and $A_-(n)$, which are the amplitudes of azimuthal waves travelling in the anti-clockwise (ACW) and clockwise (CW) directions respectively, and the spin ratio $SR(n)$ [4]. The pressure response of azimuthal mode components of order n is thus evaluated as $P'_A(n) = |A_+^2(n) + A_-^2(n)|^{1/2}$. All pressure fluctuation amplitudes are described at a reference location $x = -54$ mm. Moreover, the multi-microphone method was used to locally characterise the magnitude of acoustic velocity oscillations ($|u(t)'|$) at the dump plane ($x = 0$ mm).

The dynamics of a single flame were analysed by synchronised high speed OH* chemiluminescence imaging. A high-speed camera (Phantom V2012) with intensifier (LaVision IRO) and UV filter (centre wavelength of 310 nm and a full width at half maximum of 10 nm) was used to capture the dy-

Please cite this article as: M. Mazur, Y.H. Kwah and T. Indlekofer et al., Self-excited longitudinal and azimuthal modes in a pressurised annular combustor, Proceedings of the Combustion Institute, https://doi.org/10.1016/j.proci.2020.05.033

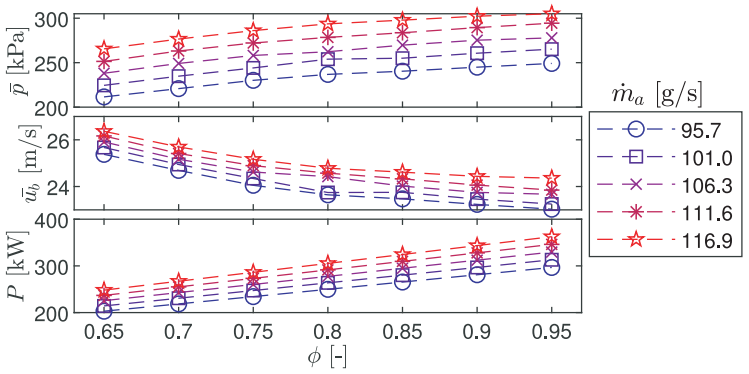

Fig. 2. Mean pressure, bulk velocity, and thermal power as functions of $\dot{m}_a$, and ϕ.

namics at angular location, $\theta = 30^\circ$. 110,000 images were acquired at 10 kHz at an image resolution of 640×528 pixels, and spatial resolution of 0.11 mm/pixel. Imaging results are presented as phase averaged intensity distributions.

3. Results and discussion

3.1. Variation of mean operating conditions

Varying $\dot{m}_a$ and ϕ for a fixed exit area results in variations of the mean pressure $\overline{p}$, defined in the injection tubes, the bulk flow velocity u_b, defined at the dump plane ($x = 0$mm), and the thermal power. As shown in Fig. 2, the pressure varies from 210 to 305 kPa, increasing with both $\dot{m}_a$ and ϕ, due to the stagnation temperature rise and choked exit boundary conditions at all operating points. While bulk inlet velocity u_b increases with $\dot{m}_a$, it slightly decreases with ϕ due to the associated pressure increase. However, the variation in bulk flow velocity is relatively narrow ($\sim 10\%$), ranging from $u_b = 23.5 - 26.2$m/s. Power increases with $\dot{m}_a$ and ϕ, and ranges from $\sim 200 - 360$ kW.

3.2. Longitudinal to azimuthal instability transition

During the experiments a variety of self-excited instabilities were observed including both longitudinal and azimuthal modes, strongly depending on operating condition. At low equivalence ratios only longitudinal modes were observed. However, at high equivalence ratios a more complicated transitional behaviour occurred, during which mode switching between longitudinal and azimuthal states was observed, accompanied by a dramatic change in flame shape due to flashback.

Fig. 3 shows mode transition for the $\phi = 0.95$, $\dot{m}_a = 116.9$g/s case through a number of metrics. The pressure time series from a single sensor at location $\theta_{k=1}$ was used to calculate the spectrogram (Hamming windows of length 98 ms, and overlap 60 %). The acoustic velocity oscillation magnitude is presented with the pressure time series, which shows the envelope of the pressure response. A time series of spin ratio is also plotted for azimuthal mode components of order $n = 1, 2$, and the flame structure is described through photographs taken with an SLR camera at selected times.

From the spectrogram, a strong longitudinal mode can be initially observed to dominate at a frequency of ~ 410 Hz. The image at time t_1 corresponds to this excitation, and a swirling bluff-body stabilised flame structure can be observed at each injector location. The flame structure is noticeably diffuse, which is due to the strong oscillations (described further in Section 3.4).

The flames are observed to flashback between time t_1 and t_2, stabilising upstream of the bluff body. Later inspection identified that the flames flash back a distance of 10mm, before anchoring on the downstream edge of the swirl vanes in each injector tube. The image at time t_2 shows the flame structure initially after flashback occurred, with a more compact structure and narrower distribution in the transverse direction. The image shown in Fig. 3 was chosen to illustrate that on occasion, not all flames flashback, which is likely due to slight imperfections in the flow uniformity from flame to flame.

Flashback occurred in response to an increase in equivalence ratio. However, over multiple repeat measurements, the time until flashback varied by up to 10 seconds, after the new operating condition had been reached. It is our conjecture that this relatively long and variable delay may be associated with thermal inertia. After ϕ is increased, the dump plane and bluff body temperatures will also increase over several seconds due to the higher thermal power, permitting flashback through the low velocity flow in the boundary layer. As shown in Fig. 2, increasing ϕ reduces the bulk flow velocity, while increasing flame speed, and although flame speed has a weak inverse scaling with pressure [21], the higher ratio of flame speed to bulk flow veloc-

Please cite this article as: M. Mazur, Y.H. Kwah and T. Indlekofer et al., Self-excited longitudinal and azimuthal modes in a pressurised annular combustor, Proceedings of the Combustion Institute, https://doi.org/10.1016/j.proci.2020.05.033

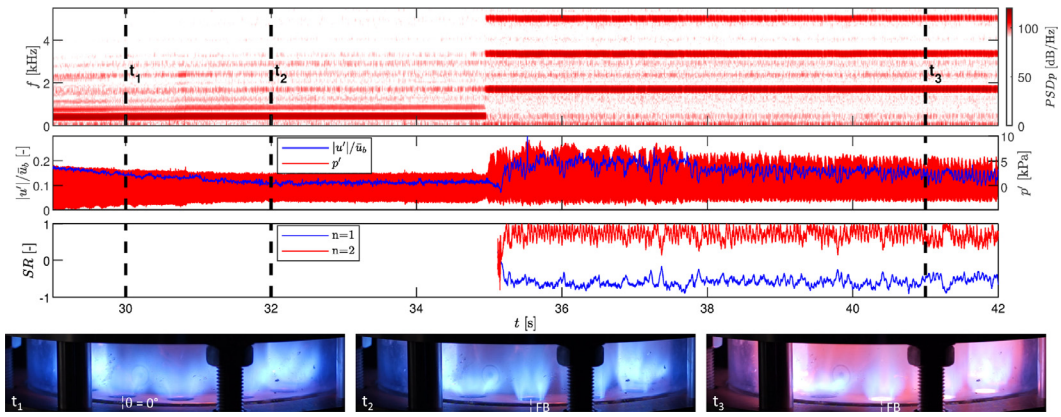

Fig. 3. Transitional behaviour of instability, switching from longitudinal to azimuthal modes for the $\phi = 0.95$, $\dot{m}_a = 116.9$ g/s case. Spectrogram (*top row*), and pressure and normalised bulk velocity oscillations (*second row*) both from $\theta_{k=1}$ location. Spin ratio time series for azimuthal modes (*second row*). Images (*bottom row*) show mean flame structure at: t_1, during longitudinal mode; t_2, flashback induced change to flame structure during longitudinal mode; t_3, after transition to azimuthal mode. FB: Flashbacked flame

ity at higher equivalence ratios ($\phi \geq 0.85$) enables flashback.

The frequency remains relatively constant prior to flashback, while the pressure oscillation amplitude decreases only slightly, but is still significant. The pressure oscillations result in significant ($|u'|/\bar{u}_b \approx 0.15$ for the $n = 1$ component) longitudinal velocity oscillations, as shown in Fig. 3. Thus, given the significant periodic oscillations in the bulk flow velocity, the flashback observed is also likely to depend on the presence of combustion instabilities in the system.

After flashback, modal transition from longitudinal to azimuthal takes place as shown in the spectrogram in Fig. 3, with the fundamental azimuthal mode component at a frequency of $f_{A,n=1} \approx 1.65$ kHz accompanied by significant amplitude higher harmonics. Following flashback, the bluff bodies undergo significant heating, as shown in the image at t_3. The notable delay of up to 5 seconds between the sudden change in flame structure following flashback, and the mode transition from longitudinal to azimuthal, we again conjecture is a result of thermal inertia.

In the example presented in Fig. 3 not all flames exhibit flashback, creating an asymmetric distribution. However, this transitional case was tested 15 times, and on a number of occasions all flames flashback. It was observed that this does not change the transition behaviour, with qualitatively similar flashback and then mode switching from longitudinal to azimuthal being observed during each repeat test. Furthermore, the nature of the azimuthal modes after switching is also qualitatively similar. Therefore, the transient phenomena described herein can be regarded as highly repeatable.

To confirm the nature of the modes observed in Fig. 3, the power spectral density was calculated separately for regions in the time series corresponding purely to longitudinal and azimuthal modes, as shown in Fig. 4, which includes local representative pressure time series to show the time dependent behaviour.

During longitudinal oscillations, time varying pressure oscillations at locations around the annulus are of similar amplitude and approximately in-phase. The pressure oscillations deviate slightly from sinusoidal behaviour due to the presence of higher harmonics, which can be clearly observed in the PSD and in the filtered time series. It is also interesting to note the presence of frequency content corresponding to the first azimuthal mode component and corresponding higher harmonics even when the longitudinal mode dominates.

In contrast, following modal transition the PSD shows only significant peaks for azimuthal mode components. The pressure time series during azimuthal instability now shows large departures from sinusoidal behaviour due to significant amplitude harmonics, which are clearly observed in the filtered time series. The filtered time series for the fundamental $n = 1$ component exhibits pressure oscillations of similar magnitude, with a phase lag corresponding to the angular separation of the sensors, indicative here of a strong CW spinning mode. Given the dominant amplitude of this fundamental component, similar features can be identified in the unfiltered pressure times series. However, the behaviour of the $n = 2$ component is distinctly different, exhibiting spinning behaviour in the ACW direction, at this instant in time. The modal dynamics are also presented later in Fig. 6, which shows that for this case, the fundamental and first harmonic spin in opposing directions. Given the current arrangement of sensors it is not pos-

Please cite this article as: M. Mazur, Y.H. Kwah and T. Indlekofer et al., Self-excited longitudinal and azimuthal modes in a pressurised annular combustor, Proceedings of the Combustion Institute, https://doi.org/10.1016/j.proci.2020.05.033

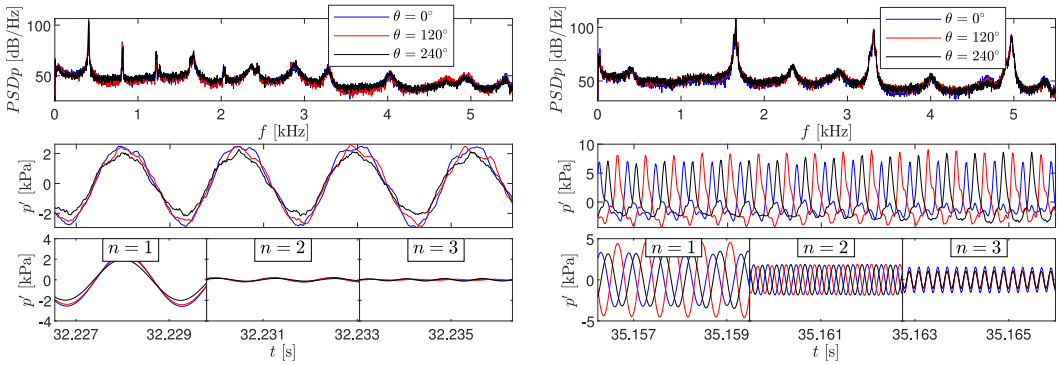

Fig. 4. Pressure PSD (*top row*) and local pressure time series during predominantly longitudinal (*LHS*) and azimuthal (*RHS*) modes for the $\phi = 0.95$, $\dot{m}_a = 116.9$g/s case, at a location $x = -54$ mm. Both unfiltered (*middle row*) and filtered (*bottom row*) pressure time series are shown.

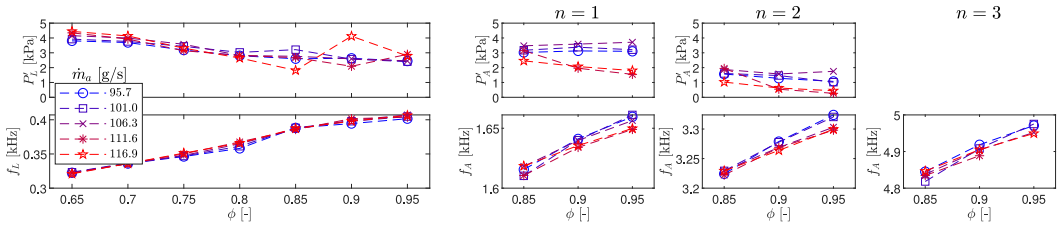

Fig. 5. Amplitude (*top row*) and frequency (*bottom row*) response of longitudinal (*LHS*) and azimuthal (*3 RHS columns*) mode components as a function of ϕ and $\dot{m}_a$, evaluated at $x = -54$ mm.

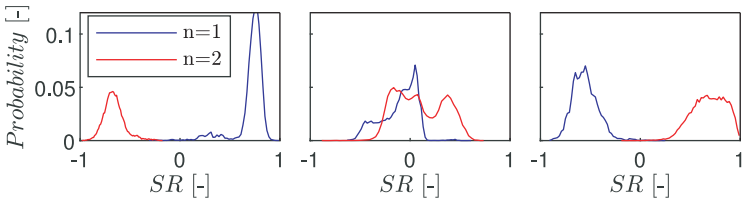

Fig. 6. *SR* probabilities for *n=1,2*. Left: $\phi = 0.85$, $\dot{m}_a = 111.6$ g/s. Middle: $\phi = 0.95$, $\dot{m}_a = 95.7$ g/s. Right: $\phi = 0.95$, $\dot{m}_a = 116.9$ g/s.

sible to determine the modal dynamics of the 2nd harmonic ($n = 3$).

3.3. Stability analysis and modal dynamics

Following the analysis of transition between longitudinal and azimuthal modes, the stability over the range of operating conditions is now described. Fig. 5 shows the frequency and amplitude response for both longitudinal and azimuthal instabilities as a function of ϕ and $\dot{m}_a$. The transitional flashback phenomena was only observed when $\phi \geq 0.85$, and azimuthal modes are thus plotted for a restricted range. The self-excitation frequency for all mode components is shown to increase with ϕ as expected, due to the increase in gas temperature and speed of sound within the combustion chamber. The lack of dependence on $\dot{m}_a$, and therefore thermal power also suggest that minor differences in wall cooling rates do not significantly affect the chamber temperature.

While the pressure response shows a weak inverse scaling with ϕ, longitudinal modes show little dependence on $\dot{m}_a$. Therefore, given the strong dependence of pressure and power on $\dot{m}_a$ shown previously in Fig. 2, the absolute magnitude of longitudinal instability does not appear to scale with these. Azimuthal mode components in contrast show some dependence on $\dot{m}_a$, with lower amplitudes observed for the two highest $\dot{m}_a$ cases. The amplitudes are of a similar order of magnitude for both longitudinal and azimuthal modes and an order of magnitude larger in absolute terms (and several times larger when normalised by the mean pressure) in comparison with similar measurements made at atmospheric conditions [3].

Please cite this article as: M. Mazur, Y.H. Kwah and T. Indlekofer et al., Self-excited longitudinal and azimuthal modes in a pressurised annular combustor, Proceedings of the Combustion Institute, https://doi.org/10.1016/j.proci.2020.05.033

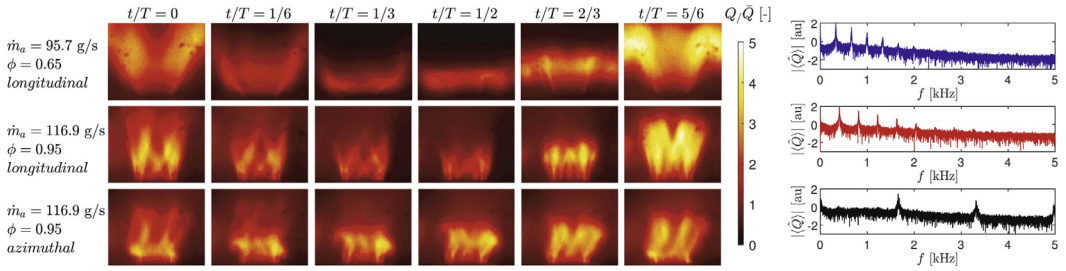

Fig. 7. Phase averaged OH* chemiluminescence imaging of a single flame at $\theta = 30^{\circ}$ (*LHS*), and frequency spectra of the globally integrated fluctuating heat release rate (*RHS*), conditioned for 3 states: $\phi = 0.65$, $\dot{m}_a = 95.7$ g/s (*Top*); $\phi = 0.95$, $\dot{m}_a = 116.9$ g/s (*midlle*) longitudinal; $\phi = 0.95$, $\dot{m}_a = 116.9$ g/s azimuthal (*bottom*).

The azimuthal modal dynamics can be assessed through the distribution of spin ratios, as shown through PDF distributions for selected cases in Fig. 6. While significant variations were observed in SR as ϕ and $\dot{m}_a$ were varied, no clear trends could be identified. However, it is interesting to note that the modal dynamics of azimuthal mode components of order, $n = 1, 2$ both demonstrate distinct modal preferences. This can result in the preferential selection of separate states. For example, the modal distribution for the $\phi = 0.85$ $\dot{m}_a = 111.6$ g/s case shows the first two azimuthal mode components select distinct spinning modes. In contrast, the components in the $\phi = 0.95$ $\dot{m}_a = 95.7$ g/s case show a preference for predominantly standing behaviour. Corresponding peak locations in this case raise the possibility of coupling between the dynamics of these components (also suggested by the time varying spin ratios shown previously in Fig. 3), and a more detailed investigation of the modal dynamics between harmonic components is warranted in future work.

3.4. Flame dynamics

Fig. 7 shows the phase averaged flame dynamics (LHS), and integrated PSD (RHS) for the three flow states described in Section 3.2. The upper row of images illustrates the $\phi = 0.65$, $\dot{m}_a = 95.7$ g/s case. Flashback was not observed and the magnitude of the longitudinal instability is associated with extreme oscillations in flame length and heat release rate through the cycle. From the point of minimum heat release rate, where the flame is flattened against the dump plane, the flame brush rolls up in response to the longitudinal velocity fluctuation, resulting in maximum heat release rate at $t/T = 5/6$.

The lower two rows correspond to the $\phi = 0.95$, $\dot{m}_a = 116.9$ g/s case after flame flashback. During longitudinal instability (middle row), oscillations in both flame length and heat release rate stay similar. However, as noted in Fig. 3, flashback results in a dramatic modification of the flame structure, reducing the spreading angle, and altering the distribution of heat release. Angled streaks of high intensity heat release rate are likely to correspond to increasing patternation from the six vane swirler, resulting in a loss of symmetry.

In the bottom row, the reduced flame brush angle and increased patternation are still present, but the azimuthal self-excitation leads to different dynamics. The flame length oscillations are now accompanied by a strong asymmetric transverse flapping motion. The strong CW spinning mode ($\overline{SR} = -0.58$) results in pressure oscillations travelling from right to left, leading to stronger vortex roll up on the left hand side, and an inclined propagation downstream of the flame brush. Due to the higher frequency of oscillation, the variation in heat release rate magnitude is less pronounced through the cycle in comparison with the longitudinal modes.

Finally, given the strong presence of higher harmonic content shown previously in Section 3.2, the magnitude of the globally integrated fluctuating heat release rate $|\langle\widehat{Q}\rangle|$ is analysed in frequency spectra, where $\langle\dots\rangle$ and $\widehat{\dots}$ denote the ensemble average and frequency space fluctuations respectively. The amplitude of the spectra is represented on a logarithmic scale. As shown on the RHS of Fig. 7, significant peaks can be seen for both longitudinal and azimuthal mode components of order $n = 1 - 3$. While the relative magnitudes of the $n = 1$ and $n = 2$ azimuthal components modes is less pronounced in comparison with the pressure response presented in Section 3.2, the magnitude of the harmonic modes is still significant, confirming the importance of these in a description of the overall response.

4. Conclusions

A new pressurised laboratory scale annular combustor was introduced and used to characterise the occurrence and dynamics of self-excited instabilities. High equivalence ratios modified the flame stabilisation location and flame structure, pro-

Please cite this article as: M. Mazur, Y.H. Kwah and T. Indlekofer et al., Self-excited longitudinal and azimuthal modes in a pressurised annular combustor, Proceedings of the Combustion Institute, https://doi.org/10.1016/j.proci.2020.05.033

moting transition from longitudinal to azimuthal modes.

The frequency and amplitude of both longitudinal and azimuthal modes were characterised across a range of mass flow rates and equivalence ratios, resulting in a variation of pressure, power and flow rate. A weak inverse scaling of amplitude with equivalence ratio was observed for the majority of modes. Additionally, significant amplitude higher order harmonics were observed for the azimuthal modes, and these were observed to contain distinct time varying modal dynamics.

Simultaneous high speed OH^* chemiluminescence measurements were also used to characterise a range of flow states, demonstrating distinct dynamics corresponding to both longitudinal and azimuthal modes. Significant higher harmonic oscillations were also observed in the heat release rate oscillations, demonstrating the response of high amplitude self-excited azimuthal instabilities under pressurised conditions may contain additional complexity in comparison with modes generated at atmospheric conditions.

Declaration of Competing Interest

None.

Acknowledgements

This work was funded by the ERC under the EU's Horizon 2020 research and innovation programme (GA no. 677931). We also acknowledge CBOne for the design and manufacture of the IPA facility.

Supplementary material

Supplementary material associated with this article can be found, in the online version, at doi:10.1016/j.proci.2020.05.033.

References

[1] W. Krebs, P. Flohr, B. Prade, S. Hoffmann, *Combust. Sc. Tech.* 174 (2002) 99–128.
[2] N.A. Worth, J.R. Dawson, *Proc. Combus. Inst.* 34 (2013) 3127–3134.
[3] N.A. Worth, J.R. Dawson, *Combustion and Flame* 160 (2012) 2476–2489.
[4] J.-F. Bourgouin, D. Durox, J.P. Moeck, T. Schuller, S. Candel, ASME Turbo Expo 2013V01BT04A007.
[5] N.A. Worth, J.R. Dawson, *Proc. Combus. Inst.* 36 (2017) 3743–3751.
[6] K. Prieur, D. Durox, T. Schuller, .S. Candel, *J. Eng. Gas Turbines Power* 140 (2017) 031503.
[7] M. Mazur, H.T. Nygård, J.R. Dawson, N.A. Worth, *Proc. Combus. Inst.* 37 (2019) 5129–5136.
[8] P. Wolf, G. Staffelbach, L.Y.M. Gicquel, J.-D. Müller, T. Poinsot, *Combustion and Flame* 159 (2012) 3398–3413.
[9] N. Zettervall, M. Mazur, J.R. Dawson, N.A. Worth, C. Fureby, *Proc. Combus. Inst.* 37 (4) (2019) 5223–5231.
[10] N. Noiray, B. Schuermans, *Proc. R. Soc. A Math. Phys. Eng. Sci.* 469 (2012).
[11] G. Ghirardo, M.P. Juniper, *Proc. R. Soc. A Math. Phys. Eng. Sci.* 469 (2013).
[12] B. Schuermans, V. Bellucci, C.O. Paschereit, *ASME Turbo Expo* (2003) 509–519.
[13] M.R. Bothien, N. Noiray, B. Schuermans, *J. Eng. Gas Turbines Power* 137 (2015) 061505.
[14] J.P. Moeck, D. Durox, T. Schuller, S. Candel, *Proc. Combus. Inst.* 37 (2019) 5343–5350.
[15] Z. Xi, Z. Fu, X. Hu, S.W. Sabir, Y. Jiang, *Energies* 11 (2018) 930–949.
[16] M. Cazalens, S. Roux, C. Sensiau, T. Poinsot, *J. Prop. Power* 24 (2008) 770–778.
[17] M. Mazur, W. Tao, P. Scouflaire, F. Richecoeur, S. Ducruix, *ASME Turbo Expo* (2015). V04BT04A001
[18] C. Lapeyre, M. Mazur, P. Scouflaire, F. Richecoeur, S. Ducruix, T. Poinsot, *Flow Turb. Combust.* 98 (2017) 265–282.
[19] M. Mastrovito, S.M. Camporeale, A. Forte, B. Fortunato, ASME Turbo Expo 2005749–756.
[20] D. Fanaca, P.R. Alamela, C. Hirsch, T. Sattelmayer, *J. Eng. Gas Turbines Power* 132 (2010) 071502.
[21] A.A. Konnov, *J. Proc. Europ. Combust. Meeting* (2015) 071502.

Please cite this article as: M. Mazur, Y.H. Kwah and T. Indlekofer et al., Self-excited longitudinal and azimuthal modes in a pressurised annular combustor, Proceedings of the Combustion Institute, https://doi.org/10.1016/j.proci.2020.05.033